Journal of Magnetic Resonance 281 (2017) 26–30

Contents lists available at ScienceDirect

Journal of Magnetic Resonance

journal homepage: www.elsevier.com/locate/jmr

Quantitative DLA-based compressed sensing for T_1-weighted acquisitions

Pavel Svehla [a,b,1], Khieu-Van Nguyen [a,b,1], Jing-Rebecca Li [c], Luisa Ciobanu [a,b,*]

[a] NeuroSpin, CEA Saclay, 91191 Gif-sur-Yvette, France
[b] University Paris-Saclay, XI, 91450 Orsay, France
[c] INRIA-Saclay, Equipe DEFI, CMAP, Ecole Polytechnique, 91128 Palaiseau, France

ARTICLE INFO

Article history:
Received 6 February 2017
Revised 5 May 2017
Accepted 7 May 2017
Available online 09 May 2017

Keywords:
Manganese-enhanced magnetic resonance imaging (MEMRI)
Compressed sensing (CS)
Diffusion limited aggregation (DLA)
Magnetic resonance microscopy (MRM)
Aplysia californica

ABSTRACT

High resolution Manganese Enhanced Magnetic Resonance Imaging (MEMRI), which uses manganese as a T_1 contrast agent, has great potential for functional imaging of live neuronal tissue at single neuron scale. However, reaching high resolutions often requires long acquisition times which can lead to reduced image quality due to sample deterioration and hardware instability. Compressed Sensing (CS) techniques offer the opportunity to significantly reduce the imaging time. The purpose of this work is to test the feasibility of CS acquisitions based on Diffusion Limited Aggregation (DLA) sampling patterns for high resolution quantitative T_1-weighted imaging. Fully encoded and DLA-CS T_1-weighted images of *Aplysia californica* neural tissue were acquired on a 17.2T MRI system. The MR signal corresponding to single, identified neurons was quantified for both versions of the T_1 weighted images. For a 50% undersampling, DLA-CS can accurately quantify signal intensities in T_1-weighted acquisitions leading to only 1.37% differences when compared to the fully encoded data, with minimal impact on image spatial resolution. In addition, we compared the conventional polynomial undersampling scheme with the DLA and showed that, for the data at hand, the latter performs better. Depending on the image signal to noise ratio, higher undersampling ratios can be used to further reduce the acquisition time in MEMRI based functional studies of living tissues.

1. Introduction

Recent advances in the static magnetic field strength of magnetic resonance scanners and in the radio-frequency (RF) detector designs has allowed magnetic resonance microscopy (MRM) to reach spatial resolutions suitable for functional imaging of single cells [1–3]. However, in order to reach the full potential of MRM it is necessary to reduce the currently long acquisition times required for obtaining high resolution images. Based on the fact that MR images, among other types of images, are compressible, an image can be reconstructed from a small number of random measurements [4]. This finding opened the field of Compressed Sensing (CS) which can significantly reduce the MRI scan time and found numerous applications in preclinical [5] and clinical [6] imaging.

In CS, high-quality images can be obtained from data sampled well below the Nyquist rate provided that the sampling pattern is incoherent, the images are sparse in a transform domain, and a sparsity-promoting iterative reconstruction is used [4]. The CS method has been previously utilized for the acceleration of T_1 weighted acquisitions for knee cartilage quantification [7] as well as for MEMRI [8]. In case of the MEMRI study, CS with random k-space undersampling patterns was employed for fast cardiac T_1 mapping in mice [8], demonstrating the feasibility and performance of this approach. Both studies used random undersampling schemes in the high frequency domain while fully sampling the low frequency domain, which has been shown to reach a similar performance to that of the polynomial undersampling algorithms [8]. Recently we have introduced a different approach for undersampling the k-space based on using the diffusion limited aggregation (DLA) random growth model to obtain reduced acquisition patterns in the phase encoding directions [9]. We have demonstrated that this DLA-CS algorithm performs better than the polynomial approach and validated its use in high resolution T_2 weighted imaging. In the present study we implement DLA-CS for T_1 weighted acquisitions in order to perform high-resolution quantitative functional MEMRI and we evaluate its performance.

* Corresponding author at: NeuroSpin, CEA Saclay, 91191 Gif-sur-Yvette, France.
E-mail address: luisa.ciobanu@cea.fr (Luisa Ciobanu).
[1] Authors who contributed equally to this work.

http://dx.doi.org/10.1016/j.jmr.2017.05.002
1090-7807/

2. Methods

2.1. Undersampling pattern generation

The undersampling pattern generation for DLA-CS RARE (Rapid Acquisition with Relaxation Enhancement) acquisitions was previously reported by Nguyen et al. [9]. Briefly, the two phase encoding directions in a Cartesian 3D trajectory were undersampled using an acquisition pattern based on the diffusion limited aggregation random growth model [10] with the k-space points in the resulting patterns always being restricted to be a subset of the fully sampled k-space points.

In this study, following the same procedure, acquisition patterns were generated for seven undersampling ratios ranging from 30% to 90% for a T_1 weighted FLASH (Fast Low Angle Shot) acquisition. For each undersampling ratio, 300 sets of undersampling patterns, each consisting of 100 candidates, were created. From each set, the one pattern (out of 100) with the lowest Point Spread Function was selected. Hence, 300 patterns were produced for each undersampling ratio, making a total of $300 \times 7 = 2100$ patterns. The 2100 patterns were applied to a library of six fully sampled T_1 weighted images of *Aplysia californica* buccal ganglia. In order to compare the CS and fully sampled images, the root mean square errors (RMSE) were calculated according to the equation:

$$RMSE = \sqrt{\frac{\sum_{i=1}^{n}(S_i - S_i')^2}{n}} \quad (1)$$

where S_i and S_i' are the signal intensities of voxel i in the fully encoded image and the undersampled image, respectively, and n is the total number of pixels. For each undersampling ratio, the averaged RMSE over the six images in the library was computed. The DLA undersampling pattern with the lowest RMSE was selected (the RMSE for the six data sets can be found in Supporting Table S1) and was implemented in Paravision 5.1 (Bruker BioSpin, Ettlingen, Germany) starting from the standard FLASH pulse sequence.

Examples of k-space undersampling patterns are shown in Fig. 1. The k-space was undersampled along the two phase encoding directions and the pattern was repeated for every point in the read direction.

For comparison, seven undersampling patterns based on the polynomial undersampling method [11] were also generated, following the same procedure.

2.2. Data acquisition

All MRI acquisitions were performed at 19 °C on a 17.2 T system (Bruker BioSpin, Ettlingen, Germany) equipped with 1 T/m gradients. The RF transceiver used for imaging was a custom-built solenoidal single-microcoil with an inner diameter of 2.4 mm, the design of which has been described previously [1]. Two types of acquisitions were performed for each sample: a RARE acquisition, providing T_2 contrast (TR = 3000 ms, TE = 20 ms, acceleration factor $A_F = 4$, 25 μm isotropic resolution, 1 average, 1 repetition) and a FLASH acquisition providing T_1 contrast (TR = 150 ms, TE = 2.441 ms, 3 averages, 2 repetitions, 25 μm isotropic resolution) in fully encoded and CS variants. The FOV was either $10 \times 2.2 \times 2.2$ mm^3 or $10 \times 2.0 \times 2.0$ mm^3 (depending on the size of the ganglia) corresponding to matrix sizes of $400 \times 88 \times 88$ and $400 \times 80 \times 80$ and fully encoded FLASH acquisition times, per repetition, of 58 and 48 min, respectively. For each sample, the RARE and FLASH acquisitions had identical FOVs. Since the FOV size was not found to influence the DLA performance, the two groups were pooled together.

2.3. Sample preparation

A total of fourteen *Aplysia californica* (*Aplysia* Resources Center, University of Miami, FL, USA) were used in this study. Images acquired on ganglia from six animals were used for generating the library necessary to optimize the DLA and polynomial based CS trajectories. Six other animals were used for acquiring fully sampled data sets. Besides providing reference images, these data sets were retrospectively undersampled in order to determine the optimal undersampling ratio. Finally, two animals were used to acquire both fully encoded and DLA-CS images. These data were also retrospectively undersampled. For all experiments the animals were food deprived for 48 h prior to the beginning of the experiment in order to increase their food seeking behavior and maximize the intracellular Mn^{2+} accumulation as described previously [2]. On the day of the experiment, the animals were injected with 100 mM $MnCl_2$ solution (500 μl per 100 g body weight; NaCl 345 mM, KCl 10 mM, $MgCl_2$ 25 mM, $MnCl_2$ 100 mM, pH = 7.5) and were left in the aquarium for 45 min with unrestricted access to food (seaweed). The animals were then anesthetized with isotonic $MgCl_2$ solution (50 ml per 100 g body weight; $MgCl_2$ 360 mM, HEPES 10 mM, pH = 7.5). Buccal ganglia were resected and inserted in 1.5 mm ID borosilicate glass capillaries (Vitro-Com, Mountain Lakes, NJ, USA) containing artificial sea water (ASW; NaCl 450 mM, KCl 10 mM, $MgCl_2$ 30 mM, $MgSO_4$ 20 mM, $CaCl_2$ 10mM, pH = 7.5) and then slid inside the transceiver for MRI. The *Aplysia* buccal ganglia contain large neurons, some of which are up to 200–300 μm in diameter [12,13] and can therefore be resolved with the spatial resolution employed here.

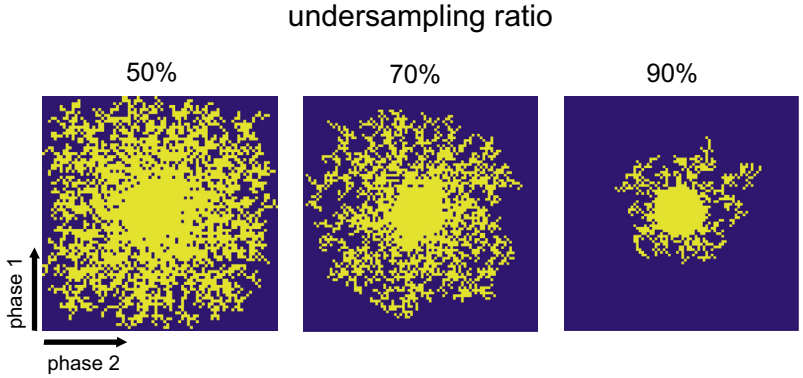

Fig. 1. DLA acquisition patterns for 50%, 70% and 90% undersampling ratios. The undersampling was performed along the two phase encoding directions.

2.4. Image reconstruction and analysis

The fully encoded images were processed directly in Paravision 5.1 software. CS undersampled data were reconstructed following the Split-Bregman algorithm provided by Goldstein and Osher in 2009 [14], which was extended for this study to a 3D version with total variation (TV) penalty and Haar wavelet transform. Briefly, if we denote the undersampled Fourier transform corresponding to the undersampled pattern F_u and W the Haar wavelet transform, the reconstructed image m is obtained by solving the following optimization problem:

$$\min_m \|Wm\|_1 + TV(m) \text{ such that } \|F_u m - f\|_2^2 < \sigma^2 \quad (2)$$

where f is the undersampled k-space data, σ is the variance of the noise and $TV(m) = \|\nabla m\|_2 = \sum_j \sqrt{(\nabla_x m_j)^2 + (\nabla_y m_j)^2 + (\nabla_z m_j)^2}$, $\nabla_i m$ representing the spatial derivative ($i = x, y, z$).

The CS reconstruction was implemented in Matlab with an approximate reconstruction time of 8 min per dataset. The original 2D reconstruction code can be found in Ref. [15].

In order to evaluate the extent of resolution loss between the fully encoded and undersampled images, we computed the Pearson's Correlation Coefficient (PCC) [16]:

$$PCC = \frac{\sum_i (S_i - S_{mean})(S'_i - S'_{mean})}{\sqrt{\sum_i (S_i - S_{mean})^2}\sqrt{\sum_i (S'_i - S'_{mean})^2}} \quad (3)$$

where S_i and S'_i represent signal intensities of voxel i in the fully encoded and retrospectively undersampled image, respectively, and S_{mean} and S'_{mean} are the corresponding mean signal intensity values over all voxels. The PCC was calculated in manually drawn ROIs containing the ganglia and encompassing approximately 50,000 voxels for both DLA and polynomial methods.

The performance of the DLA and polynomial CS strategies was further evaluated by comparing signal intensities measured in individual neurons and in water in fully encoded and retrospectively undersampled images. Five biggest neurons in the *Aplysia*'s buccal ganglia (B1, B2, B3, B6 and B9) were identified and manually segmented on RARE (T_2 weighted) images (Fig. 2a). (Note that as the buccal ganglia are bilaterally symmetric, one sample contains two neurons of each type.) The corresponding ROIs were co-registered to the FLASH (T_1 weighted) images and the mean signal intensity for each of them was calculated (Fig. 2b).

Finally, signal intensities from fully encoded and DLA prospectively undersampled T_1-weighted data sets were compared. The signal intensity quantification was performed by normalization against the water signal. To correct for possible RF inhomogeneities, the images were normalized in a position-dependent manner: the signal intensity of each voxel in the transverse plane (perpendicular to the longitudinal axis of the receiver coil) was normalized against the mean signal intensity of all voxels corresponding to ASW in this plane: $S_i^* = \frac{S_i}{S^{ASW}}$, where S_i and S_i^* are the signal intensities of voxel i before and after normalization, respectively. Details regarding this normalization procedure can be found in Ref. [2].

3. Results

Examples of fully encoded and retrospectively DLA-CS undersampled T_1 weighted images of the buccal ganglia are shown in Fig. 3. In a first step we estimated the performance of the DLA-CS

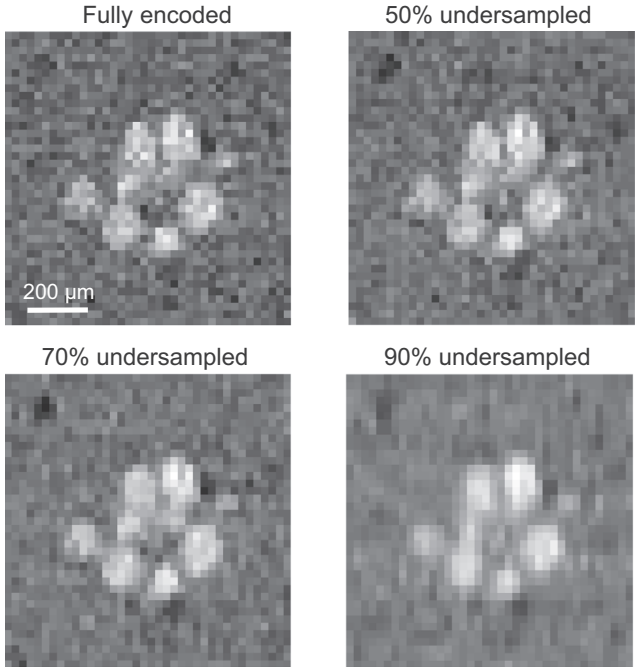

Fig. 3. Fully encoded T_1 weighted FLASH image and corresponding undersampled images after CS reconstruction (50%, 70% and 90% undersampling ratios). The CS images shown here were obtained by retrospectively undersampling the fully encoded k-space data. The hyperintense regions are neurons which accumulated Mn^{2+}. Nominal spatial resolution for the fully encoded dataset: 25 µm isotropic.

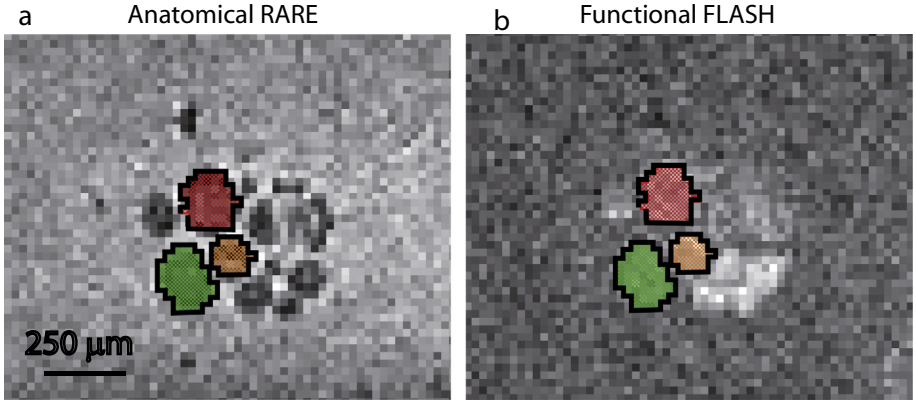

Fig. 2. Schematic representation of the ROI selection for signal intensity quantification. Two acquisitions were performed for each sample: a T_2 weighted RARE (a), providing information about the sample anatomy and a T_1 weighted FLASH (b) reflecting the intracellularly accumulated Mn^{2+} ions. Neurons were manually segmented on the RARE image and the corresponding ROIs were co-registered with the FLASH image. The drawn ROIs correspond to neurons B9 (red), B6 (orange) and B3 (green). Spatial resolution: 25 µm isotropic.

approach and compared it to polynomial CS for seven different undersampling ratios both in terms of image resolution (characterized by PCC expressing relative resolution loss between the two image sets) and relative signal intensity error (Fig. 4). As can be seen in Fig. 4a, the PCC values calculated between the CS and fully encoded images for DLA-CS undersampling are higher than those for polynomial CS, for both one and two repetitions. The PCC between the DLA-CS and fully encoded images for undersampling ratios higher than 50% drops to values below 0.8, generally considered as the threshold for a strong correlation. We observe an increase in PCC when averaging the signal over two repetitions.

The relative signal intensity error was calculated according to: $100 \times \frac{S_{mean} - S'_{mean}}{S_{mean}}$, where S_{mean} and S'_{mean} are average signal intensities, for a given ROI, in the non-normalized fully encoded images and CS images retrospectively undersampled from the same raw data set, respectively. Measurements were performed in water (water ROI) and neuron bodies (cells ROI). For the latter the signal intensities were measured in the five biggest cells (B1, B2, B3, B6 and B9) and averaged. The relative error between the average signal intensities of fully encoded and CS images, for all the undersampling ratios considered and both undersampling schemes, are displayed in Fig. 4b. DLA-CS undersampling results in lower signal intensity error than polynomial CS in the cell ROI. In addition, we notice that this error is inferior to 7% for all undersampling ratios considered. However, for undersampling ratios larger than 60% the error corresponding to the cells ROI and the water ROIs diverge, which could introduce a bias in the signal intensity quantification. The different behavior of the signal intensity error in water versus cell bodies at large undersampling ratios is most likely due to the loss in spatial resolution (increased blurring) as indicated by the PCC results (Fig. 4a). Surprisingly, the signal intensity error did not show SNR dependence (no difference between one and two repetitions). However, not only does the standard deviation of the error for the cell ROIs increase with the undersampling ratio (Fig. 4b) but we also found it to be significantly higher for one repetition when compared to two repetitions (Supporting Table S2). Specifically, a student *t*-test showed statistical significance between the SD of the signal intensity error for one and two repetitions for the cell

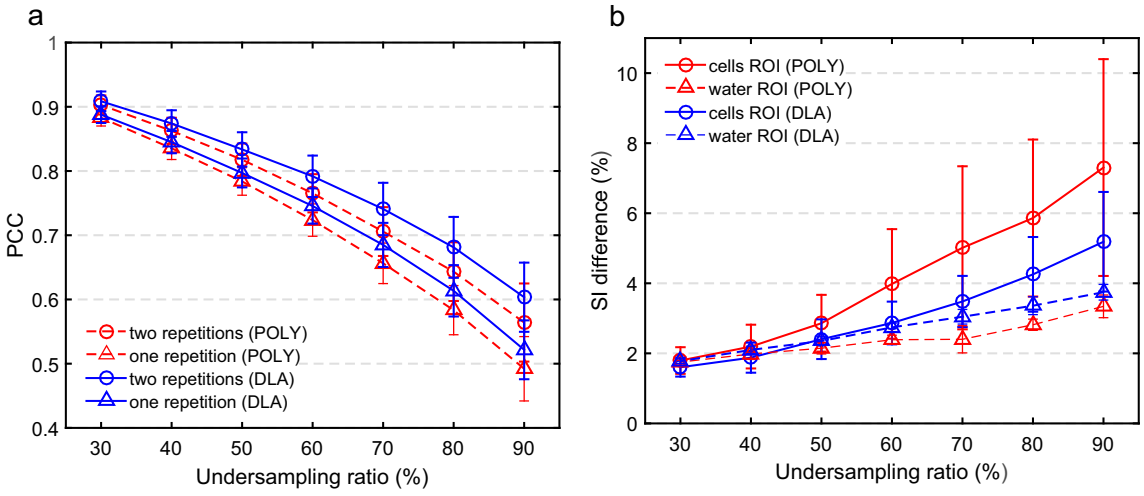

Fig. 4. Performance of DLA-CS (blue) and polynomial CS (red) for different undersampling ratios. (a) PCC between fully encoded and CS encoded images as a function of undersampling ratio for one (circle) and two (triangle) repetitions. The PCC was calculated according to Eq. (3) over the ganglia region containing approximately 50,000 voxels. Error bars represent standard deviations. (b) Percentage signal intensity difference between the fully encoded and CS images (the data represented is the average over two repetitions). Circle and triangle markers correspond to cell and water regions, respectively. Error bars represent standard deviations. The data was obtained from 6 samples.

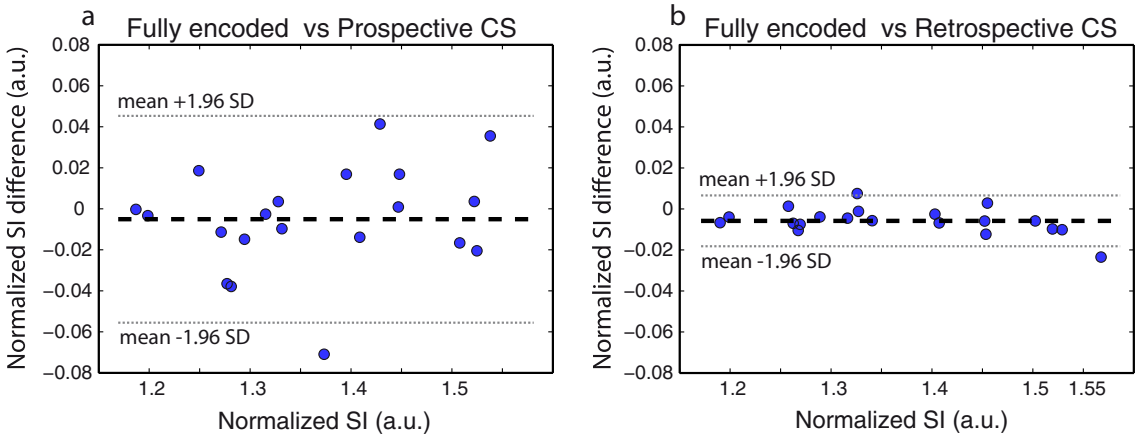

Fig. 5. Bland–Altman plots showing the difference in the normalized signal intensity values estimated from the fully sampled dataset and the 50% prospectively undersampled dataset (a) and the 50% retrospectively undersampled dataset (b). Each point corresponds to the average signal intensity measured in individual neurons (2 samples, 10 neurons per sample).

ROI ($p = 0.0005$) while for the water ROI no difference was found ($p = 0.26$).

Considering a PCC = 0.8 as the threshold for acceptable resolution loss, we chose an undersampling of 50% for the DLA pattern for our next experiments which aimed at evaluating the performance of DLA-CS acquisitions for single neuron MEMRI signal intensity quantification. The difference in the normalized signal intensity between fully encoded and compressed images was calculated for 20 neurons in two different *Aplysia* buccal ganglia (10 neurons per ganglia) according to: $S^{*}_{mean} - S^{*\prime}_{mean}$, with S^{*}_{mean} and $S^{*\prime}_{mean}$ being the average signal intensities calculated for a given ROI for fully encoded and CS images, respectively, after performing image normalization against water as described in the Methods section. The results for 50% prospectively and retrospectively undersampled datasets are shown in Fig. 5. The average difference in the normalized signal intensity values was 1.37% and 0.50% for the prospectively and retrospectively undersampled data sets, respectively.

4. Conclusion and discussion

It has been shown previously that MEMRI can be used to perform functional imaging of the buccal network of *Aplysia californica* as the manganese ions accumulate differentially in animals exposed to different food stimuli (2). The purpose of this work was to reduce the acquisition time of such MEMRI protocols by implementing DLA-CS undersampling patterns (6) and evaluate whether a quantitative analysis of the signal enhancement remains feasible. To address this issue, we obtained and compared fully encoded and DLA compressed T_1 weighted FLASH images of *Aplysia californica* buccal ganglia.

The performance of the DLA-CS FLASH acquisition was evaluated and compared to the conventional polynomial undersampling scheme at various undersampling ratios. DLA-CS undersampling was found to outperform the polynomial CS at all undersampling ratios considered in this work. When using DLA-CS, we found an undersampling ratio of 50% acceptable both in terms of image resolution and signal intensity quantification. Regarding single neuron signal intensity quantification we found, on average, a 1.37% percentage error between the fully sampled and prospectively undersampled data. This error was observed to be higher than the error measured using retrospective undersampling of the fully encoded data, which was found to be 0.50%. One of the reasons for which the retrospective CS outperforms prospective CS is that the retrospective and the fully encoded datasets share the same noise realization. In addition, the difference between the two undersampling scenarios can be also due to experimental errors such as hardware instability, subtle changes in the sample position in the B_0 field (resulting from vibrations associated with the strong encoding gradients), or slight sample modification.

When evaluating the Pearson Correlation Coefficient between the fully encoded and the undersampled images we notice that the performance of the DLA-CS technique is influenced by the image signal to noise ratio, in agreement with earlier studies [8], suggesting that higher accelerations are possible for higher SNR data.

To summarize, our results demonstrate that the DLA-CS strategy proposed here can significantly accelerate data collection in high resolution quantitative T_1-weighted FLASH acquisitions of neuronal tissues. Even though the acquisitions times remain long when compared to fast techniques, such as EPI or spiral imaging, the DLA-CS appears to be a promising approach at high magnetic fields and high spatial resolutions, where single shot acquisitions are not feasible. Moreover, the DLA-CS is not limited to magnetic resonance microscopy and could be also applied to preclinical and clinical studies, where shortening the acquisition time is equally desirable.

Acknowledgments

This work was funded by grant ANR-13-BSV5-0014-01 (project ANImE) and by the IRTELIS PhD program. The authors would like to acknowledge Boucif Djemai for assistance with animal husbandry.

Appendix A. Supplementary material

Supplementary data associated with this article can be found, in the online version, at http://dx.doi.org/10.1016/j.jmr.2017.05.002.

References

[1] I.O. Jelescu, R. Nargeot, D. Le Bihan, L. Ciobanu, Highlighting manganese dynamics in the nervous system of Aplysia californica using MEMRI at ultra-high field, Neuroimage 76 (2013) 264–271, http://dx.doi.org/10.1016/j.neuroimage.2013.03.022.
[2] G. Radecki, R. Nargeot, I.O. Jelescu, D. Le Bihan, L. Ciobanu, Functional magnetic resonance microscopy at single-cell resolution in Aplysia californica, Proc. Natl. Acad. Sci. USA 111 (2014) 8667–8672, http://dx.doi.org/10.1073/pnas.1403739111.
[3] N. Baxan, U. Kahlert, J. Maciaczyk, G. Nikkhah, J. Hennig, D. von Elverfeldt, Microcoil-based MR phase imaging and manganese enhanced microscopy of glial tumor neurospheres with direct optical correlation, Magn. Reson. Med. 68 (2012) 86–97, http://dx.doi.org/10.1002/mrm.23208.
[4] D.L. Donoho, Compressed Sens. IEEE Trans. Inf. Theory 52 (2006) 1289–1306, http://dx.doi.org/10.1109/TIT.2006.871582.
[5] C. Prieto, M.E. Andia, C. von Bary, D.C. Onthank, T. Schaeffter, R.M. Botnar, Accelerating three-dimensional molecular cardiovascular MR imaging using compressed sensing, J. Magn. Reson. Imaging JMRI 36 (2012) 1362–1371, http://dx.doi.org/10.1002/jmri.23763.
[6] O.N. Jaspan, R. Fleysher, M.L. Lipton, Compressed sensing MRI: a review of the clinical literature, Br. J. Radiol. 88 (2015) 20150487, http://dx.doi.org/10.1259/bjr.20150487.
[7] P. Pandit, J. Rivoire, K. King, X. Li, Accelerated T1 acquisition for knee cartilage quantification using compressed sensing and data-driven parallel imaging: a feasibility study, Magn. Reson. Med. 75 (2016) 1256–1261, http://dx.doi.org/10.1002/mrm.25702.
[8] W. Li, M. Griswold, X. Yu, Fast cardiac T1 mapping in mice using a model-based compressed sensing method, Magn. Reson. Med. 68 (2012) 1127–1134, http://dx.doi.org/10.1002/mrm.23323.
[9] K.-V. Nguyen, J.-R. Li, G. Radecki, L. Ciobanu, DLA based compressed sensing for high resolution MR microscopy of neuronal tissue, J. Magn. Reson. 259 (2015) 186–191, http://dx.doi.org/10.1016/j.jmr.2015.08.012.
[10] T. Witten, L. Sander, Diffusion-limited aggregation, a kinetic critical phenomenon, Phys. Rev. Lett. 47 (1981) 1400–1403, http://dx.doi.org/10.1103/PhysRevLett. 47.1400.
[11] M. Lustig, D. Donoho, J.M. Pauly, Sparse MRI: the application of compressed sensing for rapid MR imaging, Magn. Reson. Med. 58 (2007) 1182–1195, http://dx.doi.org/10.1002/mrm.21391.
[12] D. Gardner, Bilateral symmetry and interneuronal organization in the Buccal Ganglia of Aplysia, Science 173 (1971) 550–553, http://dx.doi.org/10.1126/science.173.3996.550.
[13] D. Gardner, E.R. Kandel, Diphasic postsynaptic potential: a chemical synapse capable of mediating conjoint excitation and inhibition, Science 176 (1972) 675–678, http://dx.doi.org/10.1126/science.176.4035.675.
[14] T. Goldstein, S. Osher, The split bregman method for L1-regularized problems, SIAM J. Imaging Sci. 2 (2009) 323–343, http://dx.doi.org/10.1137/080725891.
[15] Goldstein T. http://www.ece.rice.edu/~tag7/Tom_Goldstein/Split_Bregman.html.
[16] K.V. Bulusu, S. Hussain, M.W. Plesniak, Determination of secondary flow morphologies by wavelet analysis in a curved artery model with physiological inflow, Exp. Fluids 55 (2014) 1832, http://dx.doi.org/10.1007/s00348-014-1832-3.